NIH Public Access
Author Manuscript
Dev Dyn. Author manuscript; available in PMC 2015 September 01.

Published in final edited form as:
Dev Dyn. 2014 September ; 243(9): 1055–1066. doi:10.1002/dvdy.24156.

The chromatin remodeling protein CHD7, mutated in CHARGE syndrome, is necessary for proper craniofacial and tracheal development

Ethan D. Sperry[1,4,5], **Elizabeth A. Hurd**[6], **Mark A. Durham**[2], **Elyse N. Reamer**[4], **Adam B. Stein**[3], and **Donna M. Martin**[1,2,4,5,*]

[1]Department of Human Genetics, The University of Michigan, Ann Arbor, Michigan, 48109 [2]Department of Pediatrics, The University of Michigan, Ann Arbor, Michigan, 48109 [3]Department of Internal Medicine, The University of Michigan, Ann Arbor, Michigan, 48109 [4]The Medical School, The University of Michigan, Ann Arbor, Michigan, 48109 [5]The Medical Scientist Training Program, The University of Michigan, Ann Arbor, Michigan, 48109 [6]Institute of Genetics and Molecular Medicine, University of Edinburgh, Edinburgh, Scotland

Abstract

Background—Heterozygous mutations in the chromatin remodeling gene *CHD7* cause CHARGE syndrome, a developmental disorder with variable craniofacial dysmorphisms and respiratory difficulties. The molecular etiologies of these malformations are not well understood. Homozygous *Chd7* null mice die by E11, whereas $Chd7^{Gt/+}$ heterozygous null mice are a viable and excellent model of CHARGE. We explored skeletal phenotypes in $Chd7^{Gt/+}$ and *Chd7* conditional knockout mice, using *Foxg1-Cre* to delete *Chd7* (*Foxg1*-CKO) in the developing eye, ear, nose, pharyngeal pouch, forebrain, and gut and *Wnt1-Cre* (*Wnt1*-CKO) to delete *Chd7* in migrating neural crest cells.

Results—*Foxg1*-CKO mice exhibited postnatal respiratory distress and death, dysplasia of the eye, concha, and frontal bone, hypoplastic maxillary shelves and nasal epithelia, and reduced tracheal rings. *Wnt1*-CKO mice exhibited frontal and occipital bone dysplasia, hypoplasia of the maxillary shelves and mandible, and cleft palate. In contrast, heterozygous $Chd7^{Gt/+}$ mice had apparently normal skeletal development.

Conclusions—Conditional deletion of *Chd7* in ectodermal and endodermal derivatives (*Foxg1-Cre*) or migrating neural crest cells (*Wnt1-Cre*) results in varied and more severe craniofacial defects than in $Chd7^{Gt/+}$ mice. These studies indicate that CHD7 has an important, dosage-dependent role in development of several different craniofacial tissues.

Keywords

cleft palate; craniofacial disorders; skeletal dysplasia; trachea

*Correspondence to: Donna M. Martin, MD, Ph.D., 1150 W. Medical Center Dr., 3520A MSRB I, Ann Arbor, MI 48109-5652, donnamm@umich.edu, TEL: (734) 647-4859, FAX: (734) 763-9512.

NIH-PA Author Manuscript
NIH-PA Author Manuscript
NIH-PA Author Manuscript

NIH-PA Author Manuscript
NIH-PA Author Manuscript
NIH-PA Author Manuscript

Introduction

Heterozygous mutations in the gene encoding CHD7, a chromatin remodeling protein, are found in the majority of individuals diagnosed with CHARGE syndrome, a multiple anomaly disorder defined by ocular coloboma, heart defects, atresia of the choanae, retarded growth and development, genital and/or urinary abnormalities, and ear abnormalities (Janssen et al., 2012) (Janssen et al., 2012; Husu et al., 2013). Craniofacial dysmorphisms are common in CHARGE syndrome, and include square-shaped facies, facial asymmetry, external ear anomalies, cleft lip and/or palate, cranial nerve palsies, and torticollis (Zentner et al., 2010; Hughes et al., 2014). In addition, less penetrant phenotypes are associated with CHARGE and include vertebral and limb anomalies, renal anomalies, and tracheal hypoplasia or tracheo-esophageal fistula (Zentner et al., 2010; Janssen et al., 2012; Legendre et al., 2012).

Understanding the role of CHD7 during organogenesis is critical for the development of effective therapies. We have generated mouse models of CHARGE syndrome to examine molecular mechanisms of *Chd7* deficiency, including *Chd7* loss of function ($Chd7^{Gt}$) and *Chd7* conditional deletion ($Chd7^{flox}$) alleles (Hurd et al., 2007; Hurd et al., 2010). Previous studies indicate that heterozygous *Chd7* mutant mice exhibit many phenotypes similar to human CHARGE, including vestibular disorders, deafness, reduced growth, pubertal delay, olfactory dysfunction, and brain abnormalities (Bosman et al., 2005; Adams et al., 2007; Hurd et al., 2007; Layman et al., 2009; Hurd et al., 2010; Hurd et al., 2011; Layman et al., 2011; Hurd et al., 2012; Yu et al., 2013). Despite the myriad of skeletal abnormalities reported in humans with CHARGE (Prasad et al., 1997; Wright et al., 2009), there is no information about skeletal features of *Chd7* mutant mice. Because homozygous $Chd7^{Gt/Gt}$ mice do not survive beyond E11 (Bosman et al., 2005; Hurd et al., 2007), we chose to focus on $Chd7^{Gt/+}$ and *Chd7* conditional knockout mice using *Foxg1-Cre* (Hebert and McConnell, 2000) and *Wnt1-Cre* (Danielian et al., 1998) mice. The complementary expression profiles of these two different mouse lines in neural crest (*Wnt1-Cre*) and various ectodermal/endodermal derivatives (*Foxg1-Cre*) provided an opportunity to delineate the effects of loss of *Chd7* in development of various craniofacial structures.

Results

Chd7 deficient mice have craniofacial defects

The developmental origins of CHARGE-related birth defects are not fully understood. Neural crest-derived tissues are commonly affected by CHD7 deficiency (Bajpai et al., 2010), yet ectodermal structures including the brain are also affected (Legendre et al., 2012; Yu et al., 2013). In order to explore the relative contributions of CHD7 in these tissue derivatives to organ development, we generated mice with loss of *Chd7* using *Foxg1-Cre*, which is expressed by E7.5 in the pharyngeal arches, facial and head ectoderm, otic, optic, nasal and oral epithelium, pharyngeal arches, forebrain, and foregut (Hebert and McConnell, 2000). We also generated mice with *Chd7* deletion using *Wnt1-Cre*, which is expressed by E8.5 in developing pharyngeal arches, head mesenchyme, inner ear, neural crest, midbrain, spinal cord and nasal neural crest and mesenchyme (Danielian et al., 1998). Mice with

NIH-PA Author Manuscript

NIH-PA Author Manuscript

NIH-PA Author Manuscript

deletion of both *Chd7* alleles by *Foxg1-Cre* or *Wnt1-Cre* are hereafter referred to as *Foxg1*-CKO or *Wnt1*-CKO, respectively.

While $Chd7^{Gt/+}$ mice survive to adulthood (Bosman et al., 2005; Hurd et al., 2007), both *Foxg1*-CKO and *Wnt1*-CKO mice die shortly after birth, likely from respiratory failure (neither *Foxg1*-CKO nor *Wnt1*-CKO pups had milk in their stomachs). We therefore focused our phenotypic analysis of craniofacial and other tissues on postnatal day 1 pups. *Chd7* wild type, $Chd7^{flox/+}$, and $Chd7^{Gt/+}$ mice had no apparent abnormalities of the skull or craniofacial regions (Fig. 1A-B). In contrast, *Foxg1*-CKO mice had severely hypoplastic eyes (*N*=7/7 mice) and shortened faces (Fig. 1C) and *Wnt1*-CKO mice had shortened snouts (Fig. 1D). We performed comprehensive measurements of craniofacial distances on skeletal preparations of postnatal day 1 mice (Figs. 1E-H, Fig. 2 and Table 1). We observed no differences in the degree of ossification in the skulls or in craniofacial measurements (occipital bone, intersquamosal, interocular, mandible, or rostral-caudal lengths) between $Chd7^{Gt/+}$ mice and wild type or $Chd7^{flox/+}$ littermate controls (Table 1), suggesting that loss of one *Chd7* allele does not cause major or highly penetrant skeletal defects in mice. We did note mild hypoplasia of the ethmoid bone of $Chd7^{Gt/+}$ mice relative to controls (Figure 1F).

In contrast, we observed significant frontal bone dysplasia (either reduced ossification or hypoplasia) in both *Foxg1*-CKO ($N=7$, $p<0.05$) and *Wnt1*-CKO ($N=7$, $p<0.05$) mice compared with littermate controls (Figs. 1 E-H and 2 A-D). Interestingly, there was no dysplasia of the atlas (C1), axis (C2) or parietal/interparietal bones, or change in rostral-caudal lengths of $Chd7^{Gt/+}$, *Foxg1*-CKO or *Wnt1*-CKO mice compared to controls. Some mice had dysplastic ribs, but this was infrequent, also occurred in controls, and did not correlate with changes in rib number or vary significantly across genotypes. Clavicles were also normal in mice of all genotypes. Notably, the ethmoid bones were hypoplastic in both *Foxg1*-CKO and *Wnt1*-CKO mice, and the occipital region appeared dysplastic in *Wnt1*-CKO mice (Figs. 1 G, H). *Foxg1*-CKO mice exhibited significantly shortened interocular distances (mean= 3.72 vs. 4.66 mm, $N=7$, $p<0.05$) and intersquamosal distances (mean= 5.90 vs. 6.58 mm, $N=7$, $p<0.05$) compared to controls (Fig. 2C vs. A and Table 1), whereas *Wnt1*-CKO mice exhibited normal interocular or intersquamosal distances, occipital bone dysplasia and reduced mandibular length (mean=4.95 vs. 5.55 mm, $N=7$, $p<0.05$) (Fig. 2D vs. A and Table 1). Intersquamosal and interocular distances were similar in $Chd7^{Gt/+}$ mice (Fig. 2B) and controls (Fig. 2A). Thus, whereas $Chd7^{Gt/+}$ mice appear normal, both *Foxg1*-CKO and *Wnt1*-CKO mice displayed severe but distinct craniofacial anomalies, suggesting that proper *Chd7* expression within the facial ectoderm (*Foxg1*) and neural crest (*Wnt1*) is required to ensure normal craniofacial development.

Cre transgene and *Chd7* expression in developing retina correlate with ocular defects

Chd7 is expressed in mouse embryonic stem cells (Schnetz et al., 2009) and broadly in early (E7.5-E8.5) developing mouse embryos (Randall et al., 2009), then by mid-gestation (E12.5) becomes restricted to specific organs and tissues such as the brain, pituitary, ear, heart, and craniofacial structures (Hurd et al., 2007). To characterize *Chd7* expression relative to *Foxg1-Cre* and *Wnt1-Cre* transgene expression, we performed immunofluorescence for CHD7 on E11.5 transgenic embryos that also contained *ZsGreen* reporter (Madisen et al.,

NIH-PA Author Manuscript

NIH-PA Author Manuscript

NIH-PA Author Manuscript

2010) alleles (Fig. 1 I-L). CHD7 was present in the retinae of both *Foxg1-Cre;ZsGreen+* and *Wnt1-Cre;ZsGreen+* E11.5 embryos. Consistent with published results, *Foxg1-Cre*, but not *Wnt1-Cre* expression was observed in the E11.5 mouse retina (Fig. 1 J vs L) (Danielian et al., 1998; Hebert and McConnell, 2000). Thus, deletion of *Chd7* in *Foxg1*-CKO retina (with resultant hypoplastic eyes) and preservation of *Chd7* (with normal eyes) in *Wnt1*-CKO mice is expected given these expression patterns.

Foxg1-CKO mice have upper and lower airway abnormalities including conchae dysplasia and hypoplastic nasal epithelia

Individuals with CHARGE syndrome have highly penetrant respiratory and olfactory deficits, including choanal atresia, tracheoesophageal fistula, and hyposmia or anosmia (Zentner et al., 2010; Bergman et al., 2011; Layman et al., 2011). *Chd7* mutant mice are known to have severely reduced olfactory abilities and olfactory bulb hypoplasia, as well as choanal defects (Bosman et al., 2005; Layman et al., 2009; Bergman et al., 2010), but to date there is no detailed information about upper and lower airway structures. We asked whether *Chd7* heterozygous and conditional mutant mice also exhibit airway dysplasia by analyzing the structure of the oral/nasal cavity in skeletal preparations of postnatal day 1 pups. The majority of $Chd7^{Gt/+}$ mice (*N*=4/6) and all *Foxg1*-CKO (*N*=7/7) and *Wnt1*-CKO (*N*=7/7) mice displayed ventral conchae dysplasia (Fig. 2 and Table 1). Similarly, the majority of $Chd7^{Gt/+}$ mice (*N*=5/6) and all *Foxg1*-CKO (*N*=7/7) and *Wnt1*-CKO (*N*=7/7) pups displayed dorsal conchae dysplasia (Fig. 2 and Table 1). Analysis of histologically stained sections revealed normal nasal epithelial tissues in $Chd7^{Gt/+}$ and *Wnt1*-CKO mice, despite hypoplasia of the dorsal and ventral conchae in the latter (Fig. 3B and 3C). In contrast, the nasal epithelium in *Foxg1*-CKO mice was severely disorganized and hypoplastic (Fig. 3D). Comparison of X-gal staining in $Chd7^{Gt/+}$ and *Foxg1*-CKO mice (both of which contain the $Chd7^{Gt}$ allele that expresses β-galactosidase under the control of the *Chd7* promoter, (Hurd et al., 2007)) showed that *Chd7* promoter activity is preserved in the nasal epithelium of both mutants, and that unlike $Chd7^{Gt/+}$ mice which exhibit normal nasal epithelia, the *Foxg1*-CKO nasal epithelium is severely disrupted (Fig. 3E vs. 3F). Together, these data suggest that dysplasia of the nasal epithelium in mice with reduced *Chd7* may result primarily from disruption of normal *Chd7* expression in the ectoderm rather than a secondary defect in neural crest cell migration.

Foxg1-CKO and *Wnt1*-CKO mice have palatal defects

Clefting of the lip and/or palate is reported in 33-48% of individuals with CHARGE syndrome (Zentner et al., 2010; Bergman et al., 2011). In addition, approximately one-third of $Chd7^{whi/+}$ heterozygous mutant mice have cleft palates (Bosman et al., 2005). By gross morphological analysis, we found no hard or soft palatal defects in postnatal day 1 $Chd7^{Gt/+}$pups (Figs. 2F and 3B). *Foxg1*-CKO mice exhibit mild palatal shelf hypoplasia (*N*=7/7); however do not exhibit cleft palates (*N*=0/7; Table 1, Figs. 2G and 3D). By contrast, all *Wnt1*-CKO mice (*N*=7) exhibited severe palatal shelf hypoplasia and some (*N*=3/7) *Wnt1*-CKO mice displayed complete clefting of the palate resulting in an open oral/nasal pharynx (Figs. 2D, 3C and Table 1). X-gal stained sections from $Chd7^{Gt/+}$ and *Foxg1*-CKO mice, showed β-galactosidase activity (*Chd7* promoter activity) in epithelial cells lining the palatal shelves (Fig. 3E, F). Together, these data provide evidence that *Chd7* is

NIH-PA Author Manuscript

NIH-PA Author Manuscript

NIH-PA Author Manuscript

highly expressed in the nasal/oral epithelium and may contribute to disrupted palatal formation.

Absence of long bone, vertebral, clavicular, and pelvic defects in *Chd7* mutant mice

It has been proposed that CHARGE may be considered a skeletal dysplasia, with clinical reports of limb anomalies (Van de Laar et al., 2007; Wright et al., 2009), vertebral defects, and basiooccipital abnormalities (Fujita et al., 2009). We identified no visible skeletal defects in postnatal day 1 control, *Foxg1-Cre* conditional heterozygous (*Foxg1-Cre;Chd7*$^{+/flox}$), or *Wnt1-Cre* conditional heterozygous (*Wnt1-Cre;Chd7*$^{+/flox}$) mice. Likewise, lengths of bones in the upper extremity (humerus, ulna, or radius), pelvis (intercrest, interspinous, or crest-symphysis) and lower extremity (femur, tibia, or fibula) were similar in control, *Chd7* heterozygous null (*Chd7*$^{Gt/flox}$), *Foxg1*-CKO and *Wnt1*-CKO mice (data not shown). Bones from the right and left sides of the body of all mice were also similar across all genotypes, suggesting that loss of *Chd7* does not affect axial symmetry. We observed no vertebral anomalies suggestive of spinal curvature (data not shown). Analysis of the cervical spine, thoracic spine (rib count or dysplasia) and clavicle revealed no apparent differences between *Chd7*$^{Gt/+}$, *Foxg1*-CKO, *Wnt1*-CKO, and littermate control mice (Table 1). Thus, at the level of resolution possible by analysis of skeletal postnatal day 1 preparations, we found no defects in the long bones, vertebrae, clavicles, or pelvis of *Chd7* mutant mice.

Normal development of neural crest derived cardiac structures in *Wnt1-Cre* conditional mutant mice

Cardiac defects including abnormal development and septation of the conotruncus and the development of the great vessels, are present in 75-77% of individuals with CHARGE syndrome (Zentner et al., 2010; Bergman et al., 2011; Janssen et al., 2012). In mice, some *Chd7*$^{whi/+}$ embryos (heterozygous for a *Chd7* null allele) have been reported to have interventricular septal defects, body edema and cardiac insufficiency (Bosman et al., 2005). In *Wnt1-Cre* mice, *Cre*-positive neural crest cells (NCCs) migrate to the conotruncus or early cardiac outflow tract, where they participate in septation of this tract into the pulmonary and aortic outflow tracts (Jiang et al., 2000). Additionally, NCCs migrate from the posterior hindbrain into the third, fourth and sixth pharyngeal arches where they participate in the asymmetric remodeling of the pharyngeal arch arteries (PAA) into the great vessels (Hutson and Kirby, 2007). We therefore asked whether *Wnt1*-CKO mutant mice also exhibit heart defects similar to or more severe than those previously reported. In order to demonstrate whether NCC-mediated conotruncal development is impacted by *Chd7* deletion, we assessed cardiac outflow tract development in *Wnt1*-CKO embryos. At E16.5, a time point at which cardiac outflow tract septation is complete, we observed grossly normal aortic and pulmonary septation as well as normal formation of the major branches off the aorta (*N*=4 Conditional Heterozygous (CHet) (Fig. 4A), *N*=5 *Wnt1*-CKO (Fig. 4B)). Histologic analysis with H&E staining of E16.5 *Wnt1*-CHet (*N*=7; Fig. 4C) and *Wnt1*-CKO (*N*=6; Fig. 4D) hearts confirmed normal aorto-pulmonary and right-left outflow tract septation. To determine whether neural crest-mediated PAA formation was impacted by *Chd7* deletion, we assessed PAA formation at E10.5 by India ink injection in *Wnt1*-Conditional heterozygous (Fig. 4E) and *Wnt1*-CKO (Fig. 4F) mice. Third, fourth, and sixth

NIH-PA Author Manuscript

NIH-PA Author Manuscript

NIH-PA Author Manuscript

PAA formation in *Wnt1-Cre* expressing neural crest cells was unaffected by *Chd7* deletion (*N*=5 CHet, *N*=6 *Wnt1*-CKO). Thus, we found no evidence for cardiac abnormalities in mice with *Wnt1-Cre* mediated conditional deletion of one or both copies of CHD7.

Foxg1-Cre Chd7 conditional mutants have fewer tracheal rings

Other mediastinal abnormalities, including tracheoesophageal fistula and tracheal agenesis have also been reported at relatively high penetrance (19-29%) in CHARGE syndrome (Zentner et al., 2010; Bergman et al., 2011). Tracheal cartilage was readily visible in the skeletal preparations of postnatal day 1 pups, allowing us to characterize the mice for tracheal abnormalities. Interestingly, there were, on average, 17-18 tracheal rings in control mice (*N*=16), 19 in $Chd7^{Gt/+}$ mice (*N*=6), and 19 in *Wnt1*-CKO mice (*N*=7) (Fig. 5 and Table 1). In contrast, *Foxg1*-CKO mice had, on average, only 11 tracheal rings ($p<0.001$, *N*=7) (Fig. 5 and Table 1). The severe reduction in tracheal rings may represent a developmental delay or arrest of tracheal development, and could contribute to their early postnatal respiratory distress and death.

We then asked whether *Chd7* and *Wnt1-Cre/Foxg1-Cre* transgenes are expressed in the embryonic trachea proper or in surrounding mesenchymal tissues (Woo et al., 2011). As in Figs. 1 and 3, we stained cross-sections through E11.5 *Foxg1-Cre;ZsGreen*+ and *Wnt1-Cre;ZsGreen*+ embryos at the level of the mediastinum for immunofluorescence with anti-CHD7 antibody (Fig. 5E-H). We observed abundant CHD7 staining in the presumptive esophagus and trachea, with less bright label in the surrounding mesenchyme of *Foxg1-Cre;ZsGreen*+ embryos. Interestingly, *Foxg1-Cre* transgene activity was widespread in both the tracheal epithelium and surrounding mesenchymal tissues (Fig. 5E, F) whereas *Wnt1-Cre* transgene activity was restricted to the peri-tracheal mesenchyme (Fig. 5G, H). These data suggest that CHD7 is concentrated in the tracheal primordium, and is also expressed in adjacent mesenchyme, and that loss of CHD7 in the tracheal primordium leads to severely disrupted tracheal development.

Discussion

In this study, we present data showing that *Chd7* is required for certain aspects of murine craniofacial and mediastinal development; specifically, loss of *Chd7* disrupts formation of the orbit and multiple regions of the respiratory tract. By using mice expressing *Cre* recombinase in ectoderm- and endoderm-derived cells of the developing telencephalon and pharyngeal arches (*Foxg1-Cre*) and in migratory neural crest cells (*Wnt1-Cre*), we identified components of the upper and lower respiratory tracts that likely contribute to acute respiratory failure and perinatal death of *Chd7*-conditional mutant mice. Interestingly, *Chd7* is required for proper development of multiple components along the upper and lower respiratory tracts, including the nose, hard palate, and trachea. Complex malformations of each of these organs have been noted in humans with CHARGE syndrome, and postnatal respiratory distress is a common cause for early morbidity and mortality.

NIH-PA Author Manuscript

NIH-PA Author Manuscript

NIH-PA Author Manuscript

Upper and lower airway malformations with Chd7 deficiency

Nasal conchae, or turbinates, are critical for air filtration and proper formation and maintenance of the olfactory epithelium. Specifically, the conchae provide increased nasal epithelial surface area while humidifying the air, which may help protect olfactory nerve axons traveling through the cribriform plate to synapse in the olfactory bulb (Kim et al., 2003; Kastl et al., 2009). These structures develop, in part, from the ethmoid bone, a complex structure which forms the caudal nasal cavity (Jacob and Chole, 2006). We found that *Chd7*$^{Gt/+}$ mice exhibit mild hypoplasia of the dorsal and ventral conchae as well as the ethmoid bone, whereas conditional deletion of *Chd7* in *Foxg1-Cre*-expressing mice resulted in complete loss of the nasal choanae and ethmoid bone. Interestingly, *Wnt1*-CKO mice also exhibited nasal conchae and ethmoid dysplasia, with little disruption to the nasal passageways. Given the importance of the conchae in olfactory development, their disruption could worsen olfactory neuron dysfunction in *Chd7* mutant mice and contribute to previously reported hyposmia/anosmia phenotypes (Layman et al., 2009). In addition to disruption of the nasal conchae, we observed marked disruption of the nasal passageways in *Foxg1*-CKO mice, reminiscent of the posterior nasal aperture blockage or choanal atresia reported in some *Chd7*$^{whi/+}$ mice (Bosman et al., 2005). The nose, like most other craniofacial structures, is composed of facial ectoderm and migrating cranial neural crest cells, and *Chd7* may be necessary for proper integration of these cell types. Interestingly, external naris occlusion impairs nasal turbinate development in the mouse (Coppola and Craven, 2013), evidence that development of the conchae is dependent on proper airflow. We postulate that some of the nasal abnormalities observed in *Chd7* mutant mice reflect underlying contributions of *Chd7* to development of cells derived from neural crest, ectoderm, and underlying mesenchyme.

In addition to choanal atresia, other airway abnormalities such as sinus blockage, cleft palate, and laryngomalacia, are common in CHARGE syndrome (Zentner et al., 2010; Janssen et al., 2012; Hughes et al., 2014). We observed thickening and vaulting of the palatal shelves in *Foxg1*-CKO mice and complete cleft of the palate in *Wnt1*-CKO mice. In humans, highly-arched palates indicate disruptions in maxillary shelf development, are often reported following cleft palate repair, and are commonly associated with dental crowding and speech difficulties (Eppley et al., 2005; Chapman et al., 2008; Wang et al., 2009). The occurrence of highly-arched palates has been documented in individuals with CHARGE who have intact palates or following surgical repair of a cleft palate (Akisu et al., 1998). Both *Foxg1-Cre* and *Wnt1-Cre* are expressed in cells critical for maxillary development; indeed, deletions of other genes including *β-catenin* and *Bmpr1a* using these *Cre* recombinases results in mild and more severe maxillary malformations including complete aplasia (Li et al., 2011; Wang et al., 2011). Interestingly, we did not observe palatal vaulting or clefting in our *Chd7*$^{Gt/+}$ mice. This could be a result of low sample size or effects of genetic background. Cleft palate occurs in 25% of *Chd7*$^{whi/+}$ mice (Bosman et al., 2005) and 33-48% of humans with CHARGE syndrome (Zentner et al., 2010; Janssen et al., 2012). Together, these results suggest that *Chd7* plays critical roles in *Wnt1-Cre* derived cranial neural crest cells that contribute to osteogenesis and to the overlying *Foxg1-Cre* derived oral epithelium, both of which are critical for proper maxillary development (Bush and Jiang, 2012).

NIH-PA Author Manuscript

NIH-PA Author Manuscript

NIH-PA Author Manuscript

In addition to malformations of the upper airway, we observed hypoplasia of tracheal cartilaginous rings in *Foxg1*-CKO mice. This is consistent with high levels of *Cre* expression in the tracheal primordium of *Foxg1-Cre* mice. Tracheal cartilage is critical for maintaining patency of the trachea upon expiration (Doshi and Krawiec, 2007). Thus *Chd7* may play an intrinsic role in tracheal development, consistent with the tracheal abnormalities (malacia, dysgenesis, and agenesis) observed in individuals with CHARGE. The proximity of foregut derivatives to the trachea and the high incidence of tracheoesophageal fistula in CHARGE suggest that CHD7 may be important for gut development (Perl et al., 2002). Further, we observed significant, colocalized *Chd7* and *Foxg1-Cre* activity in the presumptive esophagus suggesting that development of the larygotracheal groove is critically dependent on proper expression of *Chd7*. More detailed analysis mice will be necessary to determine the extent to which *Chd7* contributes to foregut development.

Potential dual roles for Chd7 in the eye

Development of the eye involves a dual process whereby neuroectoderm forms a proto-retinal outpouching from the rostral telencephalon (Sinn and Wittbrodt, 2013). Upon contact with growing retinal tissue, the overlying surface ectoderm induces optic cup formation. The lens is the principal structure derived from the overlying surface ectoderm. Recent reports suggest that spatiotemporal localization of lens and retinal tissue is driven by neural crest cells, which themselves differentiate into the sclera separating the developing lens from the retina (Grocott et al., 2011). These neural crest cells help direct the generation of the optic cup, which involves a complex folding process resulting in formation of the choroid fissure. In the mature eye, the choroidal fissure is almost completely closed, providing continuity to the inferior iris and retina. Defects in choroidal fissure closure present as colobomata.

Ocular colobomata of the retina and/or iris, are sometimes associated with microphthalmia, occur in 75-81% of individuals with CHARGE syndrome (Zentner et al., 2010; Bergman et al., 2011). Previous studies of $Chd7^{whi/+}$ mice showed keratoconjunctivitis sicca (dry eye) (Bosman et al., 2005), but there are no reports in *Chd7* mutant mice of ocular coloboma or other major eye defects commonly seen in CHARGE syndrome. One of our most striking findings was severe hypoplasia of the eye in *Foxg1*-CKO mice. Our immunofluorescence results from E11.5 mice also demonstrate high levels of both *Foxg1-Cre* and CHD7 in retinal tissue. Notably, in addition to the high CHD7 in retina, we detected abundant CHD7 in the developing lens. We observe no obvious defects in eye development in *Wnt1*-CKO mice, suggesting that *Chd7* may have subtle or no significant functions in neural crest cells that contribute to ocular development. Recent data from zebrafish (*D. rerio*) have implicated *chd7* in the regulation of retinal cell specification (Patten et al., 2012); our data provide the first evidence that loss of *Chd7* within the retina contributes to ocular malformations in mammals. Future studies of *Chd7* function in the developing eye should help determine the mechanistic relationship between ocular hypoplasia and colobomata.

Lack of evidence for Chd7 function in cardiac neural crest cells

Fourth pharyngeal arch artery (PAA) hypoplasia and malformations of the transverse aorta and right subclavian artery (fourth PAA derivatives) have been reported in $Chd7^{whi/+}$ mice (Randall et al., 2009). Importantly, attempted rescue of these malformations using *Wnt1*-

NIH-PA Author Manuscript

NIH-PA Author Manuscript

NIH-PA Author Manuscript

Cre, expressed in neural crest cells, and a conditional *Chd7* wild-type allele was unsuccessful, suggesting minimal contributions of *Chd7* in *Wnt1-Cre* lineages to heart formation (Randall et al., 2009). Given these observations, we further explored the role of cardiac neural crest by examining conditional deletion of *Chd7* using *Wnt1-Cre*. Neither *Wnt1*-conditional heterozygous nor *Wnt1*-CKO mice exhibited any deformity in PAA development at E10.5 or in arterial branching at E16.5, consistent with minimal or no *Chd7* function in cardiac neural crest cells. Alternatively, *Wnt1-Cre* activity may be mosaic or inefficient in the cardiac neural crest. Additional studies are necessary to distinguish among these possibilities.

Development of craniofacial structures requires correct spatiotemporal Chd7 expression

Our results demonstrate that proper expression of *Chd7* is necessary for development of the craniofacial structures contributing to the upper respiratory tract and the cartilaginous rings of the trachea. Two complementary themes emerge from our data: (1) *Chd7* expression is required in the surface ectoderm, endoderm, and migrating neural crest cells which all contribute to the development of facial structures and the eye and (2) *Chd7* likely has a significant role in the development of cartilage and bone. *Foxg1-Cre* is highly expressed by E7.5 in surface ectoderm and endoderm which populate the pharyngeal arch and pouch derivatives, respectively (Hebert and McConnell, 2000). Components of the first pharyngeal arch contribute to many of the facial bones affected in *Chd7* deficient mice and humans, including the ethmoid, maxilla, and mandible (Sperber, 1989). Migrating neural crest cell populations expressing *Wnt1-Cre* invade pharyngeal arch structures and are critical for their proper specification. Loss of *Chd7* in the embryonic frog (*X. laevis*) has been reported to result in failed neural crest cell migration from the dorsal neural tube (Bajpai et al., 2010). We found that disruptions to *Chd7* in *Wnt1-Cre* expressing neural crest cells results in developmental abnormalities in the nose and palate, but not the heart. Interestingly, we observed phenotypic differences in the nose and palate between *Foxg1-CKO* and *Wnt1-CKO* mice that may reflect differences in sites or timing of *Cre* activity. In *Foxg1-Cre* mice, *Cre* is induced around E7.5, which may affect certain populations of pre-migratory neural crest cells (Nichols, 1986), whereas *Wnt1-Cre* is activated slightly later, at E8.5, in migratory neural crest (Danielian et al., 1998). Much remains to be clarified regarding how CHD7 regulates proper gene expression in both the facial ectoderm and neural crest cells that contribute to craniofacial development.

Our results highlight the potential role that CHD7 has in regulating development of bone. Interestingly, a previous report suggests that CHD7 is required for inducing *Wnt5a*-dependent osteoblastogenesis in mesenchymal stem cells (Takada et al., 2007). Indeed, these authors determined that reduction in *Chd7* mRNA levels by RNAi caused a cell fate switch leading to the accumulation of adipocytes. While this research was performed using mesoderm-derived cell populations, CHD7 may function similarly in craniofacial osteoblasts derived from cranial neural crest cells (Minoux and Rijli, 2010). Further investigation is necessary to determine the specific function(s) of CHD7 in development of craniofacial and tracheal structures affected in CHARGE syndrome.

NIH-PA Author Manuscript

NIH-PA Author Manuscript

NIH-PA Author Manuscript

Experimental Procedures

Mice

Foxg1-Cre;Chd7$^{Gt/+}$ mice and *Chd7*$^{flox/flox}$ mice were generated and genotyped as previously described (Hurd et al., 2007; Hurd et al., 2010). Specifically, these mice were maintained on a mixed C57BL/6;129S1/SvImJ background and inbred to N=6-8. Mice of the following genotypes were analyzed: control (*Chd7*$^{+/flox}$), *Chd7* heterozygous mutant (*Chd7*$^{Gt/flox}$ or *Chd7*$^{Gt/+}$), *Foxg1* conditional heterozygous mutant (*Foxg1-Cre;Chd7*$^{+/flox}$) and *Foxg1*conditional knockout mutant (*Foxg1-Cre;Chd7*$^{Gt/flox}$ or *Foxg1*-CKO). *Wnt1-Cre;Chd7*$^{+/flox}$ mice were crossed with *Chd7*$^{flox/flox}$ mice, and the following genotypes were analyzed: control (*Chd7*$^{+/flox}$ or *Chd7*$^{flox/flox}$), *Wnt1-Cre* conditional heterozygous mutant (*Wnt1-Cre;Chd7*$^{+/flox}$) and *Wnt1*conditional knockout mutant (*Wnt1-Cre;Chd7*$^{flox/flox}$ or *Wnt1*-CKO). *ZsGreen Cre* reporter mice (Madisen et al., 2010) (JAX#007906) were crossed with *Foxg1-Cre* or *Wnt1-Cre* mice to identify sites of *Cre* positive cells. The University of Michigan University Committee on the Use and Care of Animals (UCUCA) approved all procedures.

Skeletal Preparations

Postnatal day 1 mice were terminally anaesthetized, eviscerated, and fixed in 95% ethanol overnight and incubated in acetone for three days. Preparations were placed in dye solution (0.06 mg/ml Alizarin Red (Sigma, St. Louis, MO) and 0.18 mg/mL Alcian Blue (Sigma) in 42 mL of 72% ethanol and 3 mL of glacial acetic acid) and agitated gently on a rotary shaker for four days. Skeletons were washed in ddH_2O for two hours to rinse excess dye then placed in 1% KOH clearing solution for two days. Samples were then immersed in increasing concentrations of glycerol (1:4 glycerol / 1% KOH; 1:1 glycerol / 1% KOH; 8:2 glycerol / 1% KOH) for five to seven days per immersion. Finally, skeletal preparations were stored in 100% glycerol, photographed using a Leica DMRB microscope and measured using ImageJ (National Institutes of Health, Bethesda, MD). Images were processed using Adobe Photoshop CS6 (Adobe, San Jose, CA).

Histology and X-gal staining

Postnatal day 1 mice were collected, decapitated and heads fixed in 4% paraformaldehyde overnight at 4°C. After washing in PBS, heads were incubated in 30% sucrose, embedded in OCT medium (Tissue-Tek, Torrance, CA), frozen, and sectioned at 12-15 μm. Sections were either stained with hematoxylin and eosin (H&E) (Sigma) for histological analysis, or X-gal for expression analysis as previously described (Hurd et al., 2007). Sections were photographed by light microscopy on a Leica upright DMRB microscope and processed in Photoshop CS2 (Adobe, San Jose, CA).

Immunofluorescence and Cre lineage tracing

For *Cre* lineage tracing and anti-CHD7 immunofluorescence, E11.5 *Foxg1-Cre;ZsGreen;Chd7*$^{+/+}$ and *Wnt1-Cre;ZsGreen;Chd7*$^{+/+}$ embryos were harvested, dissected, and embedded in OCT cryosectioning media (Tissue-Tek, Torrance, CA). Embryos were cryosectioned at 14 μm, stained with 1:7500 anti-CHD7 rabbit IgG monoclonal antibody (in

NIH-PA Author Manuscript

NIH-PA Author Manuscript

NIH-PA Author Manuscript

TSA block, #6505 Cell Signaling Technology (Danvers, MA) and counterstained with 1:200 biotinylated anti-rabbit IgG goat secondary antibody (in TSA block, BA-1000, Vector Laboratories (Burlingame, CA)). Strepavidin-HRP (1:100 in TSA block) was added to slides and Alexa 555 tyramide (1:100 in Amplification Buffer, Molecular Probes (Grand Island, NY)) was applied to generate fluorescence. DAPI (5 μg/mL) was added and slides mounted for imaging using a Leica DMRB microscope. Final image processing was performed using Adobe Photoshop CS6 (Adobe, San Jose, CA).

Cardiac Evaluation

For gross inspection, E16.5 embryos were harvested and dissected. For the hematoxylin/eosin stained sections, embryos were fixed in 4% paraformaldehyde for 12–18 hours at 4°C, dehydrated and embedded in Leica Histowax according to standard procedures. After embedding, sections were cut at 5–7 μm. Images were analyzed by brightfield microscopy. For India ink injections, E10.5 embryos were dissected and placed in ice cold PBS. Using a pulled glass pipette, India ink was injected into the ventricles until the ink penetrated the small vessels. Embryos were post-fixed in 10% buffered formalin for 12 hours, dehydrated and cleared in benzylbenzoate: benzyl alcohol (2:1v/v).

Statistical analysis

Measurements of anatomical regions were performed on control (*N*=16), *Chd7* heterozygous mutant (*N*=6), *Foxg1* conditional heterozygous mutant (*N*=7), *Wnt1* conditional heterozygous mutant (*N*=2), *Foxg1* conditional knockout mutant (*N*=7) and *Wnt1* conditional knockout mutant (*N*=7) mice using stereoscope-standardized pictures analyzed with ImageJ (National Institutes of Health, Bethesda, MD). Discrete observations (i.e. presence or absence of dysplasia) were scored in a binomial fashion. Bone lengths were measured using ImageJ (National Institutes of Health, Bethesda, MD). All measurements were analyzed in SPSS (v.19.0) by MANOVA with a *post hoc* Tukey's honest significant difference (HSD) test; significance was limited to $p \leq 0.05$.

Acknowledgments

We thank John L. Zeller, M.D., Ph.D. (Division of Anatomical Sciences, University of Michigan) for assistance with interpretation of skeletal anatomy. This work was supported by the CHARGE Syndrome Foundation (EAH and ABS), Elizabeth E. Kennedy Research Award (EAH), Hearing Health Foundation (EAH), and NIH grants 5T32GM007863-33 (EDS), 5T35GL007690-30 (ENR), and R01-DC009410 (DMM).

Grant Sponsor: NIH R01-DC009410.

References

Adams ME, Hurd EA, Beyer LA, Swiderski DL, Raphael Y, Martin DM. Defects in vestibular sensory epithelia and innervation in mice with loss of Chd7 function: implications for human CHARGE syndrome. J Comp Neurol. 2007; 504:519–532. [PubMed: 17701983]

Akisu M, Ozkinay F, Ozyurek R, Kucuktas A, Kultursay N. The CHARGE association in a newborn infant. Turk J Pediatr. 1998; 40:283–287. [PubMed: 9714686]

Bajpai R, Chen DA, Rada-Iglesias A, Zhang J, Xiong Y, Helms J, Chang CP, Zhao Y, Swigut T, Wysocka J. CHD7 cooperates with PBAF to control multipotent neural crest formation. Nature. 2010; 463:958–962. [PubMed: 20130577]

NIH-PA Author Manuscript

NIH-PA Author Manuscript

NIH-PA Author Manuscript

Bergman JEH, Bosman EA, van Ravenswaaij-Arts CMA, Steel KP. Study of smell and reproductive organs in a mouse model for CHARGE syndrome. European Journal of Human Genetics. 2010; 18:171–177. [PubMed: 19809474]

Bergman JEH, Janssen N, Hoefsloot LH, Jongmans MCJ, Hofstra RMW, van Ravenswaaij-Arts CMA. CHD7 mutations and CHARGE syndrome: the clinical implications of an expanding phenotype. Journal of Medical Genetics. 2011; 48:334–342. [PubMed: 21378379]

Bosman EA, Penn AC, Ambrose JC, Kettleborough R, Stemple DL, Steel KP. Multiple mutations in mouse Chd7 provide models for CHARGE syndrome. Hum Mol Genet. 2005; 14:3463–3476. [PubMed: 16207732]

Bush JO, Jiang R. Palatogenesis: morphogenetic and molecular mechanisms of secondary palate development. Development. 2012; 139:231–243. [PubMed: 22186724]

Chapman KL, Hardin-Jones MA, Goldstein JA, Halter KA, Havlik RJ, Schulte J. Timing of palatal surgery and speech outcome. Cleft Palate Craniofac J. 2008; 45:297–308. [PubMed: 18452355]

Coppola D, Craven B. The effects of naris occlusion on mouse nasal turbinate development. J Exp Biol. 2013

Danielian PS, Muccino D, Rowitch DH, Michael SK, McMahon AP. Modification of gene activity in mouse embryos in utero by a tamoxifen-inducible form of Cre recombinase. Curr Biol. 1998; 8:1323–1326. [PubMed: 9843687]

Doshi J, Krawiec ME. Clinical manifestations of airway malacia in young children. J Allergy Clin Immunol. 2007; 120:1276–1278. [PubMed: 18073123]

Eppley BL, van Aalst JA, Robey A, Havlik RJ, Sadove AM. The spectrum of orofacial clefting. Plast Reconstr Surg. 2005; 115:101e–114e.

Fujita K, Aida N, Asakura Y, Kurosawa K, Niwa T, Muroya K, Adachi M, Nishimura G, Inoue T. Abnormal basiocciput development in CHARGE syndrome. AJNR Am J Neuroradiol. 2009; 30:629–634. [PubMed: 19112063]

Grocott T, Johnson S, Bailey AP, Streit A. Neural crest cells organize the eye via TGF-beta and canonical Wnt signalling. Nat Commun. 2011; 2:265. [PubMed: 21468017]

Hebert JM, McConnell SK. Targeting of cre to the Foxg1 (BF-1) locus mediates loxP recombination in the telencephalon and other developing head structures. Dev Biol. 2000; 222:296–306. [PubMed: 10837119]

Hughes SS, Welsh HI, Safina NP, Bejaoui K, Ardinger HH. Family history and clefting as major criteria for CHARGE syndrome. Am J Med Genet A. 2014; 164A:48–53. [PubMed: 24214489]

Hurd EA, Adams ME, Layman WS, Swiderski DL, Beyer LA, Halsey KE, Benson JM, Gong TW, Dolan DF, Raphael Y, Martin DM. Mature middle and inner ears express Chd7 and exhibit distinctive pathologies in a mouse model of CHARGE syndrome. Hear Res. 2011

Hurd EA, Capers PL, Blauwkamp MN, Adams ME, Raphael Y, Poucher HK, Martin DM. Loss of Chd7 function in gene-trapped reporter mice is embryonic lethal and associated with severe defects in multiple developing tissues. Mamm Genome. 2007; 18:94–104. [PubMed: 17334657]

Hurd EA, Micucci JA, Reamer EN, Martin DM. Delayed fusion and altered gene expression contribute to semicircular canal defects in Chd7 deficient mice. Mech Dev. 2012

Hurd EA, Poucher HK, Cheng K, Raphael Y, Martin DM. The ATP-dependent chromatin remodeling enzyme CHD7 regulates pro-neural gene expression and neurogenesis in the inner ear. Development. 2010; 137:3139–3150. [PubMed: 20736290]

Husu E, Hove HD, Farholt S, Bille M, Tranebjaerg L, Vogel I, Kreiborg S. Phenotype in 18 Danish subjects with genetically verified CHARGE syndrome. Clin Genet. 2013; 83:125–134. [PubMed: 22462537]

Hutson MR, Kirby ML. Model systems for the study of heart development and disease. Cardiac neural crest and conotruncal malformations. Semin Cell Dev Biol. 2007; 18:101–110. [PubMed: 17224285]

Jacob A, Chole RA. Survey anatomy of the paranasal sinuses in the normal mouse. Laryngoscope. 2006; 116:558–563. [PubMed: 16585859]

Janssen N, Bergman JE, Swertz MA, Tranebjaerg L, Lodahl M, Schoots J, Hofstra RM, van Ravenswaaij-Arts CM, Hoefsloot LH. Mutation update on the CHD7 gene involved in CHARGE syndrome. Hum Mutat. 2012; 33:1149–1160. [PubMed: 22461308]

NIH-PA Author Manuscript

NIH-PA Author Manuscript

NIH-PA Author Manuscript

Jiang X, Rowitch DH, Soriano P, McMahon AP, Sucov HM. Fate of the mammalian cardiac neural crest. Development. 2000; 127:1607–1616. [PubMed: 10725237]

Kastl KG, Rettinger G, Keck T. The impact of nasal surgery on air-conditioning of the nasal airways. Rhinology. 2009; 47:237–241. [PubMed: 19839243]

Kim KS, Choi YS, Kim HJ, Yoon JH. The risk of olfactory disturbance from conchal plate injury during ethmoidectomy. Am J Rhinol. 2003; 17:307–310. [PubMed: 14599135]

Layman WS, Hurd EA, Martin DM. Reproductive dysfunction and decreased GnRH neurogenesis in a mouse model of CHARGE syndrome. Hum Mol Genet. 2011; 20:3138–3150. [PubMed: 21596839]

Layman WS, McEwen DP, Beyer LA, Lalani SR, Fernbach SD, Oh E, Swaroop A, Hegg CC, Raphael Y, Martens JR, Martin DM. Defects in neural stem cell proliferation and olfaction in Chd7 deficient mice indicate a mechanism for hyposmia in human CHARGE syndrome. Hum Mol Genet. 2009; 18:1909–1923. [PubMed: 19279158]

Legendre M, Gonzales M, Goudefroye G, Bilan F, Parisot P, Perez MJ, Bonniere M, Bessieres B, Martinovic J, Delezoide AL, Jossic F, Fallet-Bianco C, Bucourt M, Tantau J, Loget P, Loeuillet L, Laurent N, Leroy B, Salhi H, Bigi N, Rouleau C, Guimiot F, Quelin C, Bazin A, Alby C, Ichkou A, Gesny R, Kitzis A, Ville Y, Lyonnet S, Razavi F, Gilbert-Dussardier B, Vekemans M, Attie-Bitach T. Antenatal spectrum of CHARGE syndrome in 40 fetuses with CHD7 mutations. J Med Genet. 2012

Li L, Lin M, Wang Y, Cserjesi P, Chen Z, Chen Y. BmprIa is required in mesenchymal tissue and has limited redundant function with BmprIb in tooth and palate development. Dev Biol. 2011; 349:451–461. [PubMed: 21034733]

Madisen L, Zwingman TA, Sunkin SM, Oh SW, Zariwala HA, Gu H, Ng LL, Palmiter RD, Hawrylycz MJ, Jones AR, Lein ES, Zeng H. A robust and high-throughput Cre reporting and characterization system for the whole mouse brain. Nat Neurosci. 2010; 13:133–140. [PubMed: 20023653]

Minoux M, Rijli FM. Molecular mechanisms of cranial neural crest cell migration and patterning in craniofacial development. Development. 2010; 137:2605–2621. [PubMed: 20663816]

Nichols DH. Formation and distribution of neural crest mesenchyme to the first pharyngeal arch region of the mouse embryo. Am J Anat. 1986; 176:221–231. [PubMed: 3739949]

Patten SA, Jacobs-McDaniels NL, Zaouter C, Drapeau P, Albertson RC, Moldovan F. Role of Chd7 in zebrafish: a model for CHARGE syndrome. PLoS One. 2012; 7:e31650. [PubMed: 22363697]

Perl AK, Wert SE, Nagy A, Lobe CG, Whitsett JA. Early restriction of peripheral and proximal cell lineages during formation of the lung. Proc Natl Acad Sci U S A. 2002; 99:10482–10487. [PubMed: 12145322]

Prasad C, Quackenbush EJ, Whiteman D, Korf B. Limb anomalies in DiGeorge and CHARGE syndromes. Am J Med Genet. 1997; 68:179–181. [PubMed: 9028454]

Randall V, McCue K, Roberts C, Kyriakopoulou V, Beddow S, Barrett AN, Vitelli F, Prescott K, Shaw-Smith C, Devriendt K, Bosman E, Steffes G, Steel KP, Simrick S, Basson MA, Illingworth E, Scambler PJ. Great vessel development requires biallelic expression of Chd7 and Tbx1 in pharyngeal ectoderm in mice. J Clin Invest. 2009; 119:3301–3310. [PubMed: 19855134]

Schnetz MP, Bartels CF, Shastri K, Balasubramanian D, Zentner GE, Balaji R, Zhang X, Song L, Wang Z, Laframboise T, Crawford GE, Scacheri PC. Genomic distribution of CHD7 on chromatin tracks H3K4 methylation patterns. Genome Res. 2009; 19:590–601. [PubMed: 19251738]

Sinn R, Wittbrodt J. An eye on eye development. Mech Dev. 2013; 130:347–358. [PubMed: 23684892]

Sperber, GH. Craniofacial Embryology. Great Britain: Wright; 1989.

Takada I, Mihara M, Suzawa M, Ohtake F, Kobayashi S, Igarashi M, Youn MY, Takeyama K, Nakamura T, Mezaki Y, Takezawa S, Yogiashi Y, Kitagawa H, Yamada G, Takada S, Minami Y, Shibuya H, Matsumoto K, Kato S. A histone lysine methyltransferase activated by non-canonical Wnt signalling suppresses PPAR-gamma transactivation. Nat Cell Biol. 2007; 9:1273–1285. [PubMed: 17952062]

Van de Laar I, Dooijes D, Hoefsloot L, Simon M, Hoogeboom J, Devriendt K. Limb anomalies in patients with CHARGE syndrome: an expansion of the phenotype. Am J Med Genet A. 2007; 143A:2712–2715. [PubMed: 17937444]

NIH-PA Author Manuscript

NIH-PA Author Manuscript

NIH-PA Author Manuscript

Wang XX, Wang X, Li ZL, Yi B, Liang C, Jia YL, Zou BS. Anterior maxillary segmental distraction for correction of maxillary hypoplasia and dental crowding in cleft palate patients: a preliminary report. Int J Oral Maxillofac Surg. 2009; 38:1237–1243. [PubMed: 19720499]

Wang Y, Song L, Zhou CJ. The canonical Wnt/beta-catenin signaling pathway regulates Fgf signaling for early facial development. Dev Biol. 2011; 349:250–260. [PubMed: 21070765]

Woo J, Miletich I, Kim BM, Sharpe PT, Shivdasani RA. Barx1-mediated inhibition of Wnt signaling in the mouse thoracic foregut controls tracheo-esophageal septation and epithelial differentiation. PLoS One. 2011; 6:e22493. [PubMed: 21799872]

Wright EM, O'Connor R, Kerr BA. Radial aplasia in CHARGE syndrome: a new association. Eur J Med Genet. 2009; 52:239–241. [PubMed: 19375527]

Yu T, Meiners LC, Danielsen K, Wong MT, Bowler T, Reinberg D, Scambler PJ, van Ravenswaaij-Arts CM, Basson MA. Deregulated FGF and homeotic gene expression underlies cerebellar vermis hypoplasia in CHARGE syndrome. Elife. 2013; 2:e01305. [PubMed: 24368733]

Zentner GE, Layman WS, Martin DM, Scacheri PC. Molecular and phenotypic aspects of CHD7 mutation in CHARGE syndrome. Am J Med Genet A. 2010; 152A:674–686. [PubMed: 20186815]

NIH-PA Author Manuscript
NIH-PA Author Manuscript
NIH-PA Author Manuscript

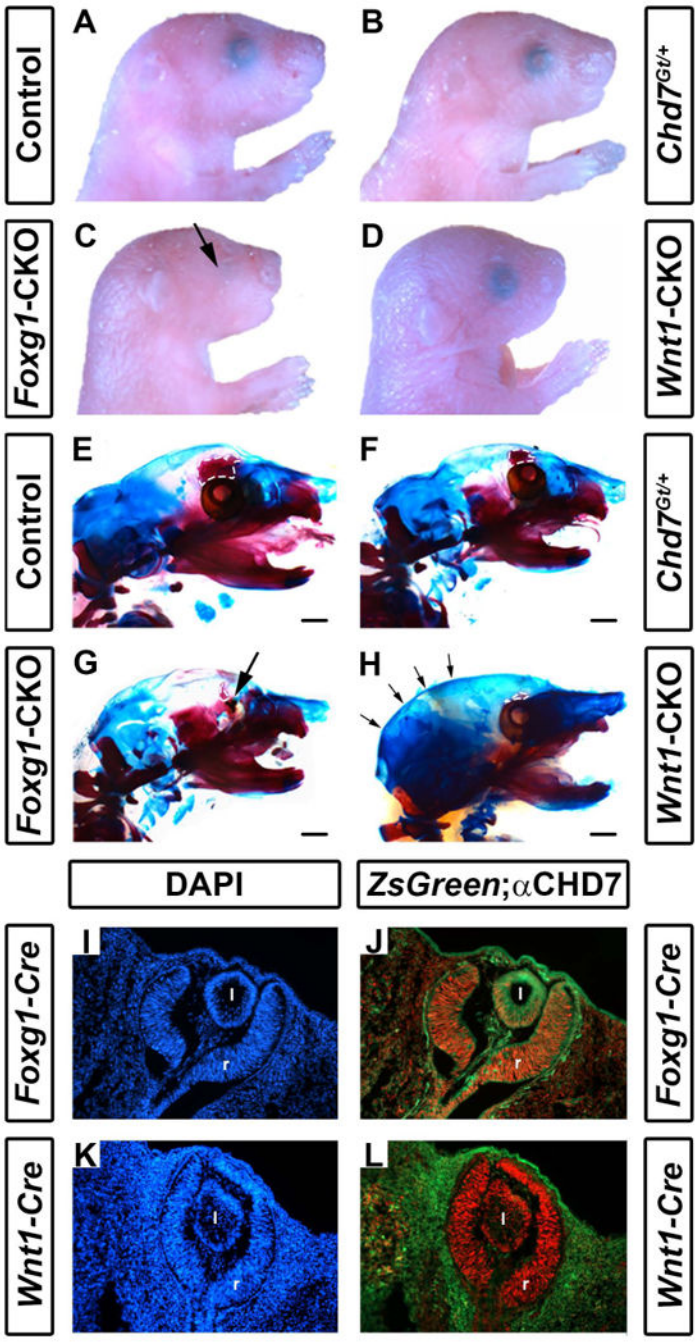

Figure 1.

Conditional deletion of *Chd7* results in ocular hypoplasia and cranial bone dysplasia. Brightfield images (A-D) and skeletal preparations (E-H) of postnatal day 1 control (*Cre*-negative, $Chd7^{+/f}$ or $Chd7^{f/f}$) (A,E), $Chd7^{Gt/+}$ (B,F), *Foxg1*-CKO (C,G) and *Wnt1*-CKO (D,H) pups. $Chd7^{Gt/+}$ mice appear similar to controls, whereas both *Foxg1*-CKO (C) and *Wnt1*-CKO (D) mice have shortened snouts, and *Foxg1*-CKO mice have ocular hypoplasia (arrows in C and G). There are no abnormalities in ossification, overall morphology or size of major craniofacial bones in $Chd7^{Gt/+}$ mice (B, F). In E-H, alizarin red and alcian blue

staining reveal bone and cartilage, respectively. Ethmoid bones are hypoplastic in *Chd7*$^{Gt/+}$ (F), *Foxg1*-CKO (G) and *Wnt1*-CKO (H) mice (white dashed lines in E-H). *Wnt1*-CKO mice (H) have a more rounded posterior cranium (indicated by arrows) than mice of other genotypes. *Cre* expression in *Foxg1-Cre* and *Wnt1-Cre* mice was detected using ZsGreen reporter mice and compared to CHD7 protein levels in the developing eye (I-L). Shown are transverse sections of *Cre;ZsGreen* positive E11.5 embryos stained with DAPI (labels cellular nuclei) or anti-CHD7 (red). *Foxg1-Cre* is active in CHD7-positive cells in the retina (r) and posterior lens (l) of the developing eye (J), whereas *Wnt1-Cre* is restricted to the surrounding periocular mesenchyme and is absent in the retina and lens proper (L). Scale bars in E-H are 1 mm.

NIH-PA Author Manuscript
NIH-PA Author Manuscript
NIH-PA Author Manuscript

NIH-PA Author Manuscript
NIH-PA Author Manuscript
NIH-PA Author Manuscript

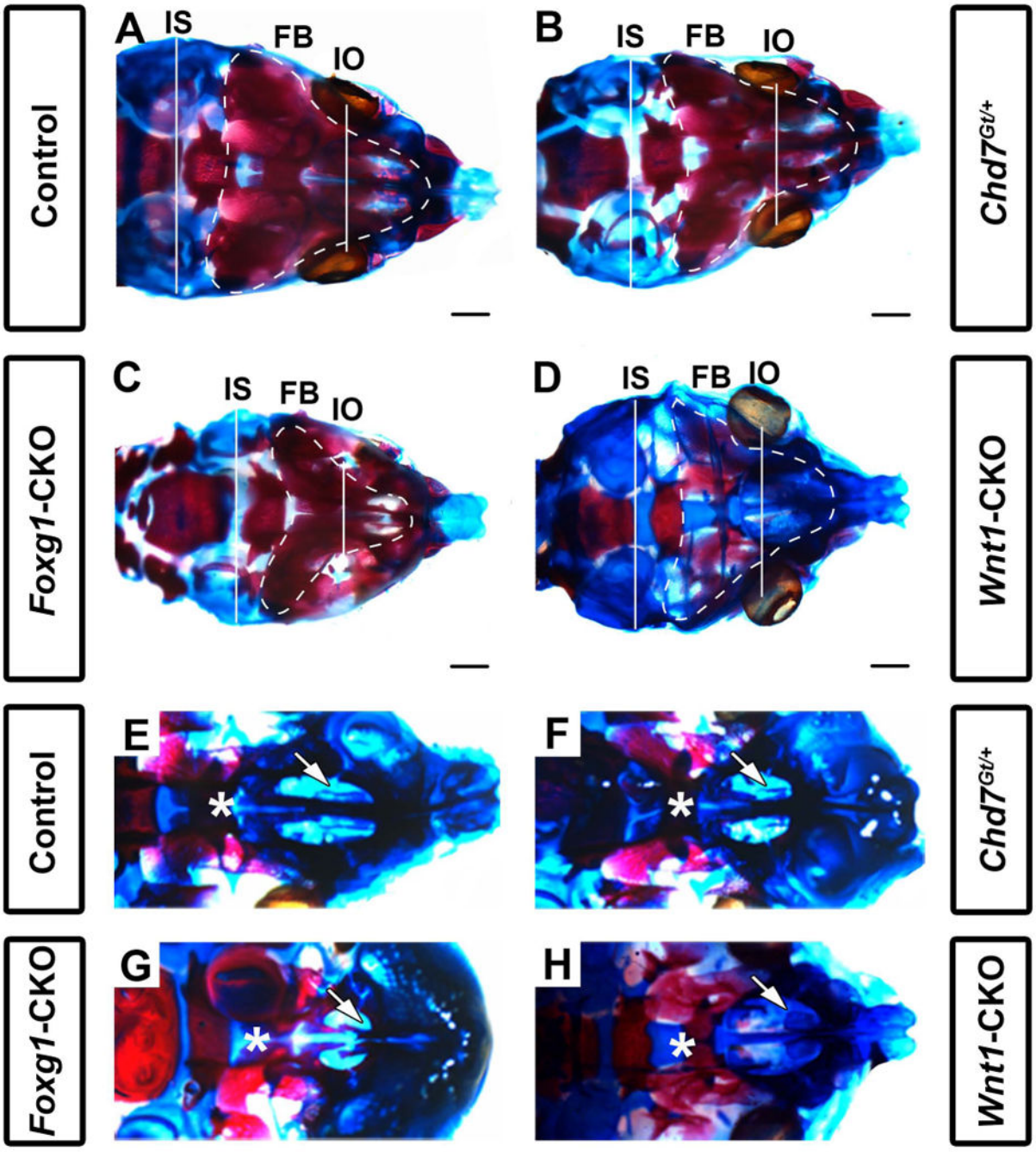

Figure 2.

Chd7 conditional mutants have shortened intraocular and intersquamosal distances, hypoplasia of the maxillary shelves, and dysplasia of nasal conchae. Skeletal preparations of postnatal day 1 control (*Cre*-negative, $Chd7^{Gt/+}$ or $Chd7^{f/f}$) (A,E), $Chd7^{Gt/+}$ (B,F), *Foxg1*-CKO (C,G), and *Wnt1*-CKO (D,H) mice. Alizarin red and alcian blue staining show bone and cartilage, respectively. (A-D) are representative dorsal images of the calvaria while (E-H) are representative dorsal images of the developing maxillary shelves (with mandibles removed). *Foxg1*-CKO (C) mice exhibit shorter interocular (white line, IO; $p<0.001$, $N=7$)

NIH-PA Author Manuscript

NIH-PA Author Manuscript

NIH-PA Author Manuscript

and intersquamosal (white line, IS; $p<0.001$, $N=7$) distances compared to control (A), *Chd7*$^{Gt/+}$ (B), and *Wnt1*-CKO (D) mice. *Foxg1*-CKO (C) mice exhibit a visibly smaller frontal bone (FB) surface area (white, dotted line) relative to control (A), *Chd7*$^{Gt/+}$ (B), and *Wnt1*-CKO (D) mice. *Wnt1*-CKO (D) mice lack frontal bone ossification (as demonstrated by alizarin red staining) relative to control (A), *Chd7*$^{Gt/+}$ (B), and *Foxg1*-CKO (C) mice. In control (E) and *Chd7*$^{Gt/+}$ (F) mice, appropriately formed palatal shelves (asterisk) and ventral nasal conchae (white arrow) are present. *Foxg1*-CKO (G) mice have hypoplastic palatal shelves which approximate the midline (asterisk) and absent ventral conchae (white arrow), whereas *Wnt1*-CKO (H) mice have severe palatal shelf hypoplasia (asterisk) and dysplastic ventral conchae (white arrow). Scale bars in A-D are 1 mm.

NIH-PA Author Manuscript
NIH-PA Author Manuscript
NIH-PA Author Manuscript

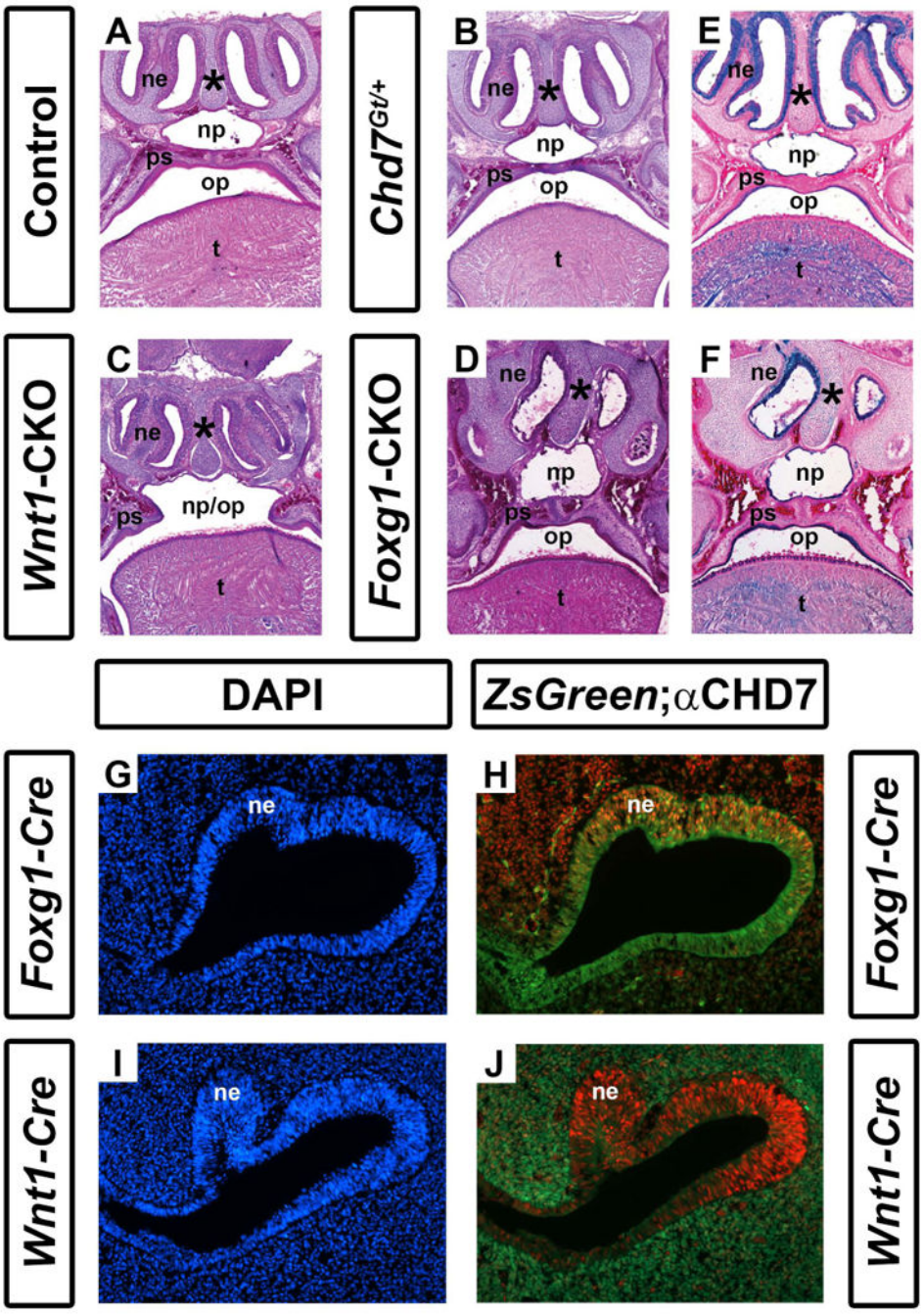

Figure 3.

Conditional *Chd7* deletion results in palatal and nasal epithelial dysplasia. Transverse sections of postnatal day 1 control (*Cre*-negative, $Chd7^{+/f}$ or $Chd7^{f/f}$) (A), $Chd7^{Gt/+}$ (B), *Wnt1*-CKO (C), and *Foxg1*-CKO (D) mice stained with hematoxylin and eosin. Control (A) and $Chd7^{Gt/+}$ (B) mice exhibit fully fused palatal shelves (ps) with separation of the nasopharynx (np) from the oropharynx (op), whereas *Wnt1*-CKO(C) mice have severely hypoplastic palatal shelves (ps) resulting in a cleft palate and single pharyngeal cavity (np/op). *Foxg1*-CKO mice (D) have fused palatal shelves (ps) resulting in a highly-arched, intact

NIH-PA Author Manuscript

NIH-PA Author Manuscript

NIH-PA Author Manuscript

palate , a thickened nasal septum (asterisk), and severely hypoplastic nasal epithelia (ne). (E) and (F) show X-gal/eosin stained sections of postnatal day 1 *Chd7*^{Gt} mice, which express β-galactosidase under the control of the *Chd7* promoter. X-gal staining is present in the nasal epithelium (ne), tongue (t) and epithelial cells lining the palatal shelves and combined oral-nasal pharynx (op/np) of *Chd7*$^{Gt/flox}$ (E) and *Foxg1*-CKO (F) mice. Panels (G-J) are transverse sections of *Foxg1-Cre;ZsGreen* (G, H) or *Wnt1-Cre;ZsGreen* (I, J) E11.5 embryos stained with DAPI (blue, marking cellular nuclei) or anti-CHD7 (red). Green fluorescence (*ZsGreen* reporter) marks *Cre* expressing cells and is overlaid with anti-CHD7 (red) in (H) and (J). *Foxg1-Cre* and *Chd7* are both highly expressed in the developing nasal epithelium (ne) while *Wnt1-Cre* expression is restricted to the surrounding nasal mesenchyme (m) and is absent from the nasal epithelium proper.

NIH-PA Author Manuscript
NIH-PA Author Manuscript
NIH-PA Author Manuscript

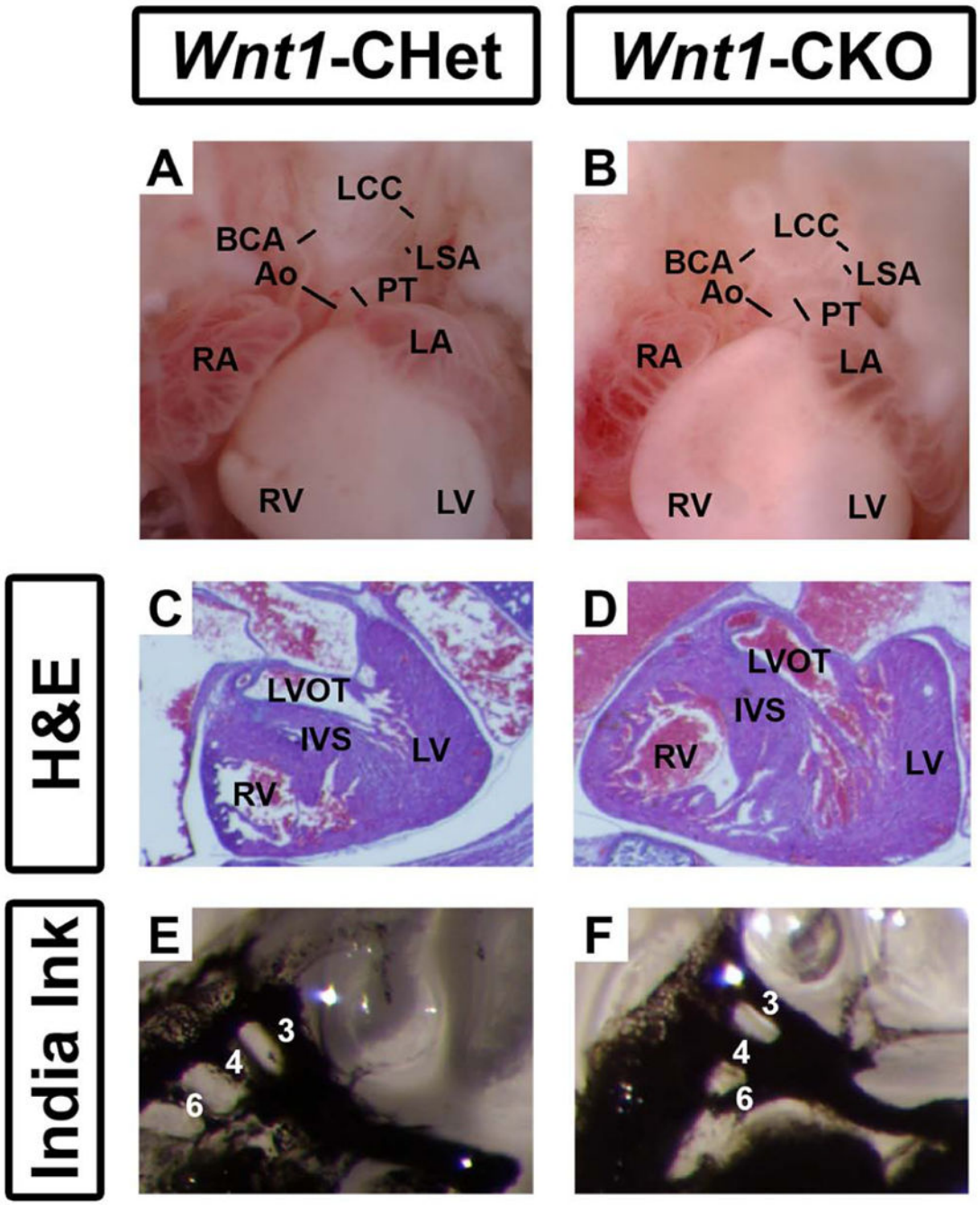

Figure 4.

Neural crest-derived cardiac structures develop normally in *Wnt1*-CHet and *Wnt1*-CKO mice. (A) E16.5 embryonic hearts from *Wnt1*-CHet and *Wnt1*-CKO embryos exhibited normal septation of the aorta (Ao) and pulmonary trunk (PT) with normal extension of the brachiocephalic (BCA), left common carotid (LCC), and left subclavian (LSA) arteries from the aortic arch. H&E staining of sectioned E16.5 embryonic hearts from *Wnt1-Cre* conditional heterozygous (B) and *Wnt1*-CKO (C) mice revealed normal development of the left ventricular outflow tract (LVOT) and inter ventricular septum (IVS). India ink injections

NIH-PA Author Manuscript

NIH-PA Author Manuscript

NIH-PA Author Manuscript

of E10.5 *Wnt1-Cre* conditional heterozygous (CHet) (D) and *Wnt1*-CKO (E) mice demonstrate normal development of the 3rd, 4th, and 6th pharyngeal arch arteries. Other abbreviations: RA (right atrium); LV (left ventricle); RA (right atrium); LA (left atrium). Lines span lumina of arteries.

NIH-PA Author Manuscript
NIH-PA Author Manuscript
NIH-PA Author Manuscript

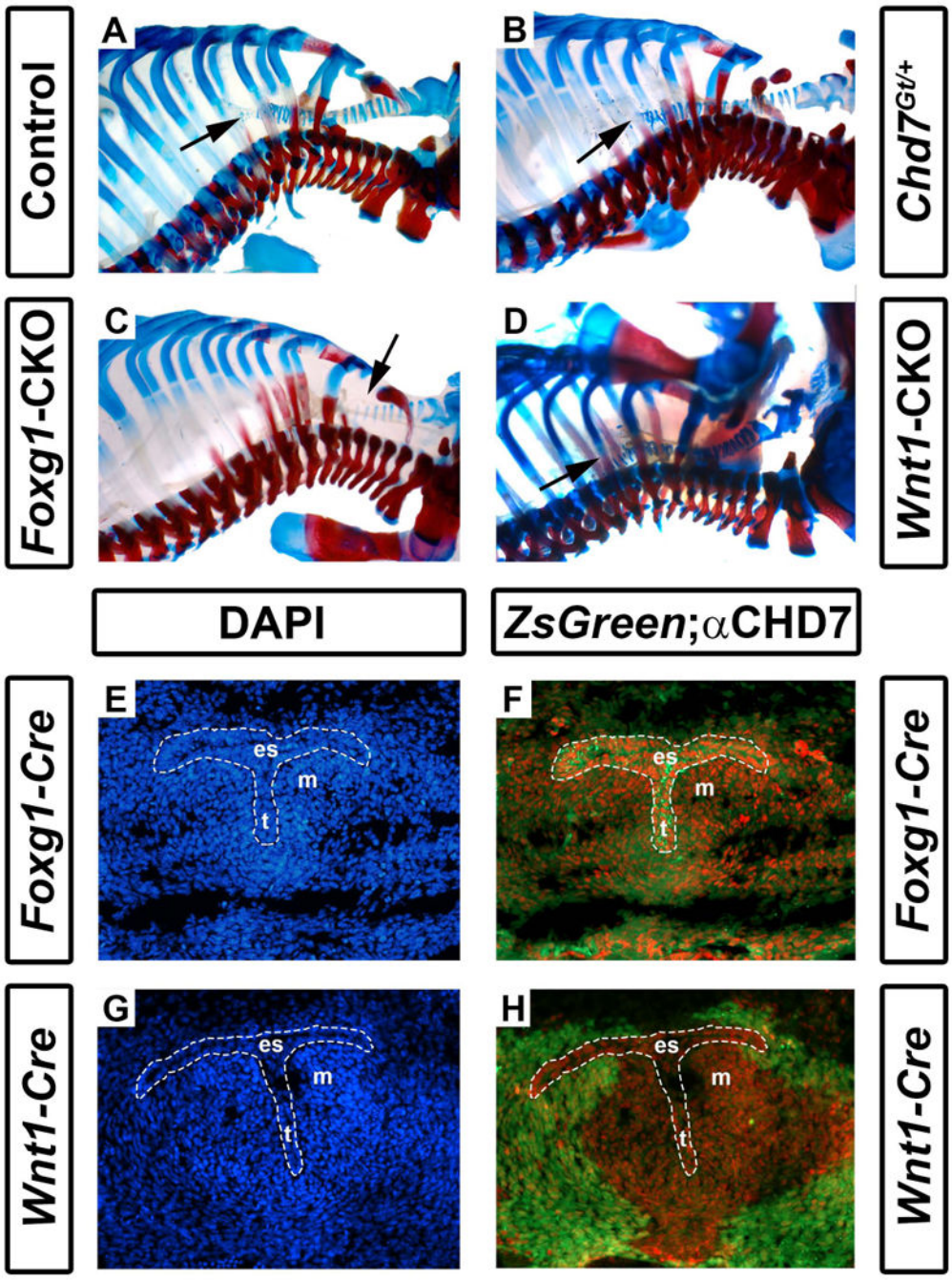

Figure 5.

Foxg1-CKO mice have reduced numbers of cartilaginous tracheal rings. Shown are skeletal preparations of postnatal day 1 control (*Cre*-negative, $Chd7^{+/f}$ or $Chd7^{f/f}$) (A), $Chd7^{Gt/+}$ (B), *Foxg1*-CKO (C), and *Wnt1*-CKO (D) mice. Alizarin red and alcian blue staining reveal bone and cartilage, respectively. Normal numbers of tracheal rings (17-19) (arrows point to distal trachea) are present in control, $Chd7^{Gt/+}$, and *Wnt1*-CKO mice, whereas *Foxg1*-CKO mice have fewer (11) tracheal rings. Panels E-H are transverse sections of *Foxg1-Cre;ZsGreen* (E, F) or *Wnt1-Cre;ZsGreen* (G, H) E11.5 embryos at the level of the laryngotracheal

NIH-PA Author Manuscript

NIH-PA Author Manuscript

NIH-PA Author Manuscript

groove (indicated by the area within the dashed white lines) stained with DAPI (blue, labeling cellular nuclei) or anti-CHD7 (red). Green fluorescence (*ZsGreen* reporter) marks *Cre*-expressing cells and is overlaid with anti-CHD7 (red) in (F) and (H). *Chd7* and *Foxg1-Cre* are highly co-expressed in the developing esophagus (es), trachea (t), and the surrounding mesenchyme (m), whereas *Wnt1-Cre* activity is restricted to the surrounding mesenchymal tissues and does not overlap with *Chd7* expression in the presumptive esophagus or trachea.

NIH-PA Author Manuscript NIH-PA Author Manuscript NIH-PA Author Manuscript

Dev Dyn. Author manuscript; available in PMC 2015 September 01.

Table 1

Foxg1-Cre or *Wnt1-Cre* conditional loss of *Chd7* in mice results in multiple skeletal abnormalities.

Region	Feature	*Foxg1-Cre* Genotype			*Wnt1-Cre* Genotype	
		Chd7$^{+/flox}$ (*N*=9)	*Chd7*$^{Gt/flox}$ (*N*=6)	CKO (*N*=7)	Control (*N*=6)	CKO (*N*=7)
Cranium	Interocular distance	4.66	4.34	3.72 *	5.12	5.01
	Frontal bone dysplasia†	3	4	7 *	0	6 *
	Eye dysplasia†	0	0	7 *	0	0
	Intersquamosal distance	6.58	6.38	5.90 *	6.23	6.24
	Parietal/interparietal bone dysplasia†	0	0	0	0	0
	Occipital bone length	3.92	4.10	3.86	3.58	3.47
	Occipital bone dysplasia†	0	0	0	1	7 *
	Rostral-caudal length	9.54	9.27	8.99	9.75	9.46
	Ventral conchae dysplasia†	0	4 *	7 *	1	7 *
	Dorsal conchae dysplasia†	0	5 *	7 *	1	7 *
	Palatal shelf dysplasia†	0	0	7*	1	7 *
	Cleft palate†	0	0	0	0	3 *
	Mandible length	5.29	5.28	5.05	5.55	4.95 *
Cervical spine	Atlas (C1) dysplasia†	0	0	0	0	0
	Axis (C2) dysplasia†	0	0	0	0	2
Thoracic spine	Rib count	13.0	13.0	12.9	12.9	12.9
	Rib dysplasia (bifid)†	1	3	1	2	4
Thorax	Clavicle length	2.49	2.49	2.48	2.60	2.56
	Tracheal ring count	17.8	19.3	11.0 *	16.7	18.9

All measurements are in millimeters.

† These observations were scored in a binomial fashion (e.g. dysplasia of the frontal bone was identified as “present” or “absent”). As such, the number of mice affected is scored across each genotype for each observation.

NIH-PA Author Manuscript

NIH-PA Author Manuscript

NIH-PA Author Manuscript

* Significance indicated at $p < 0.05$ relative to $Chd7^{+/flox}$ (for *Foxg1-Cre*) or control($Chd7^{+/flox}$ or $Chd7^{flox/flox}$ for *Wnt1-Cre*) by MANOVA with *post hoc* Tukey's HSD test.